THE BELL SYSTEM
TECHNICAL JOURNAL

VOLUME XXXVI JULY 1957 NUMBER 4

Noise Spectrum of Electron Beam in Longitudinal Magnetic Field

By W. W. Rigrod

(Manuscript received January 21, 1957)

Measurements of induced noise currents along drifting cylindrical electron beams have shown that noise fluctuations propagate as space-charge waves in the same fashion as RF signals of the same frequency. On many such beams, however, the regular standing-wave noise pattern is interrupted, after some drift distance, by a smooth steep increase in noise current, followed by slow, shallow undulations. This "growing noise" phenomenon, discovered by Smullin and his co-workers at M.I.T. several years ago, is the subject of study in this paper. Its importance is considerable, in a negative way, because it has hampered the development of medium-power traveling-wave-tube devices with acceptably low noise figures.

The experimental measurements show the growing noise pattern to be the result of a two-stage process. Its primary cause is rippled-beam amplification of noise fluctuations over a wide band of microwave frequencies, much higher than the usual observation frequency. This explains its elusiveness. In the second stage, noise energy is transferred to lower frequencies, due to intermodulation and other non-linear processes within the gain band. As the beat-frequency noise increments are excited by continuous arrays of frequency pairs, their standing-wave patterns overlap one another, resulting in a smooth growing-noise pattern.

In Part II of this paper, measurements of the noise spectrum of a rippled beam in the UHF region are described. These measurements reveal the presence of additional forms of instability. Calculations are made to account for some of these, and for aspects of rippled-beam amplification not previously understood.

Part I — The Growing Noise Phenomenon*

I INTRODUCTION

When an RF probe is moved along a magnetically-focused electron beam in a drift region, the noise power is at first found to vary periodically with distance from the electron gun.[1] For a sufficiently long beam, however, the periodic pattern is succeeded by an exponential rise, culminating in an irregular plateau. This so-called "growing noise" phenomenon has been extensively investigated by its discoverers, L. Smullin and his colleagues at the M.I.T. Research Laboratory of Electronics.[2, 3] They have established that this noise will begin to grow at a plane nearer the gun, and tend to grow at a faster rate, for electron beams (a) of higher perveance, (b) with less space-charge neutralization by positive ions, and (c) issuing from convergent, partly-shielded guns, rather than those immersed in the magnetic field.

The growth of microwave noise power in drifting beams has hampered the development of high-power, traveling-wave tubes with acceptably low noise figures, as such devices generally have convergent, partly-shielded electron guns. The problem has been evaded in the design of low-noise, low-power traveling-wave tubes, by resort to confined-flow, parallel beams.

Several theories have been proposed to explain the growing-noise wave:

(1) Excitation of higher-order modes with complex propagation constants, by electrons threading the beam transversely;[4]

(2) Slipping-stream amplification, due to either longitudinal or transverse velocity gradients;[5]

(3) Rippled-beam amplification;[6, 7, 8] and

(4) Electron-electron interactions leading eventually to equipartition of thermal energy, and thus an increase in longitudinal velocity fluctuations.

In Part I of this paper, measurements are presented which show that the principal cause of growing noise appears to be space-charge wave

* Presented at the I.R.E. Electron Tube Research Conference, Boulder, Colorado, June 27–29, 1956.

amplification due to beam rippling. The mechanism is studied in some detail, as its connection with the usually-observed exponential rise of noise is not immediately apparent. In Part II, the UHF noise spectrum and its spatial distribution in beams with large-amplitude, long wavelength ripples, are described. In addition, some of the underlying processes are analyzed.

II APPARATUS

As sketched in Fig. 1, the heart of the apparatus consists of an electron gun, drift tube, and movable probe, all enclosed in a demountable, continuously-pumped vacuum system. Outside of the vacuum envelope there is a shielded solenoid, extending the entire 18-inch length of the drift tube. The annular gap between the solenoid pole face and the magnetic shield about the gun is nearly all taken up by a soft-steel section of the vacuum envelope.

The electron gun is of the convergent Pierce type, with oxide-coated cathode and a coiled-coil filament heater producing negligible flux at the cathode surface. Surrounding the gun, and inside of the magnetic shield, is a small copper-wire coil that permits variation of this flux over a small range, either aiding or opposing the leakage flux due to the main focusing solenoid. The flux density at the cathode has been approximately calibrated in terms of currents in both coils. Throughout the experiments described below, the gun is pulsed with a 1,000 cps square wave of 2,200 volts on its anode, supplying 38 $\pm$ 1 ma peak current in space-charge-limited emission.

The novel feature of the probe is that its annular RF pickup gap couples to a 50-ohm coaxial line leading to the receiver, rather than to a resonant cavity. This permits RF power measurements over a wide range of frequencies. The inner conductor of the coaxial line serves as current-collector, being isolated and biased positively about 40 volts with respect to the outer conductor to prevent escape of slow secondaries. An adjustable vane can be locked in position in front of the probe (whose entrance aperture is 0.100 inch in diameter), so that circular apertures of various smaller sizes are fixed on the probe centerline, about 0.070 inch in front of the probe. With these apertures, measurements of collector-current variations along the beam furnish a rough picture of beam-ripple amplitudes and locations. In addition, the current-density variation across the beam can be estimated by moving a pinhole aperture in a broad arc through the beam centerline. Both the inner conductor of the probe and the intercepting vane are liquid-cooled.

The noise powers coupled to the coaxial probe are considerably smaller

than for a tuned coaxial cavity, because of the lower RF gap impedance of the former. To compensate for this drawback, a sensitive noise receiver is employed, similar in principle to the radiometer invented by R. H. Dicke.[9] The input noise power is replaced periodically by a matched load at room temperature by pulsing the beam on and off with a 1,000 cps square wave, and placing an isolator in front of the receiver. A synchronous detector eliminates gain-fluctuation noise and converts the receiver output to a dc voltage.

Noise power variations at various microwave frequencies are measured in terms of the changes of attenuation, between probe and receiver, required to keep the receiver output constant. These rapid adjustments in attenuation are performed by a servo amplifier-motor loop, and recorded on a chart, whose speed ($1\frac{1}{2}$ inches per minute) is synchronized with that of the moving probe. In the same way, records of collector current as a function of probe position can be obtained, and correlated with those of noise power. The probe can be moved a distance of about 17 inches, its position nearest the gun ($z = 0$ inches) corresponding to a distance of 0.95 inch between the anode and the input plane of the RF gap.

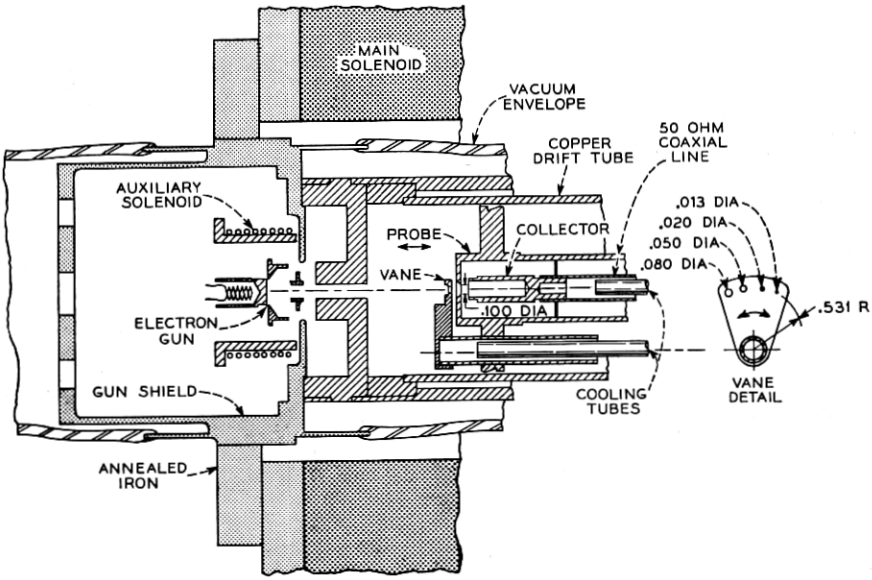

FIG. 1 — Cross-section of experimental tube, showing electron gun, probe, and two solenoids. The isolated current-collector electrode serves as inner conductor of a coaxial line. The induced RF power can be measured over a wide range of frequencies.

III EXPLORATORY MEASUREMENTS

The electron gun used in these experiments had been designed for use in a helix traveling-wave tube with a longitudinal focusing field of 600 gauss. Noise-power and collector-current curves, therefore, were first taken with 600 gauss to study a typical state of affairs in an operational beam. As seen in Fig. 2, the noise power at 3.9 kmc varies periodically with distance for about 4 inches from the gun, then climbs rather smoothly by nearly 23 db to an irregular plateau, where it undulates slowly, and finally levels off. The initial part of the growing noise curve at 10.7 kmc is missing because of inadequate receiver sensitivity, but its later portion is similar to that at 3.9 kmc, with about half the rate of noise climb. With the 0.020-inch aperture, the collector-current variations decrease in amplitude chiefly in the drift region preceding the noise climb; whereas those for the 0.100-inch aperture decrease afterwards. Both curves show a flattening in the growing-noise region itself, as well as a decrease in their *average* values after that region, signifying an increase in the average beam diameter.

A similar set of curves is shown in Fig. 3, for a focusing field of 279 gauss (about twice the nominal Brillouin field). Noise growth at 3.9 kmc starts later, and proceeds less steeply, than at 600 gauss. The noise-power curve for 10.7 kmc is much more articulated, with a semblance of periodicity, throughout the drift region. Collector-current curves for both 0.020- and 0.050-inch apertures show considerable reduction in current-ripple amplitude with distance, reaching virtually zero in the former case.

Another type of survey measurement is illustrated in Fig. 4. With the probe stationary at the far end of the drift space (about 18 inches from the gun anode), the main solenoid current is varied smoothly to change the focusing field from 0 to over 600 gauss, and synchronized records are made of collector current and noise power. (In this instance, the current in the auxiliary solenoid was +3.2 amperes.) At low magnetic fields, both the current and noise-power curves have large amplitude variations, which diminish as the field increase. At first glance, the noise peaks and valleys seem to coincide with those of collector current; certainly, some do. Closer inspection, however, reveals significant misalignments which cannot be accounted for by experimental error. When the three noise curves, at 3,050, 3,930, and 4,730 mc, respectively, are compared with each other, some characteristic features emerge:

(1) An average curve drawn through each pattern has one or two broad maxima, which tend to move toward higher field strengths with increasing frequency.

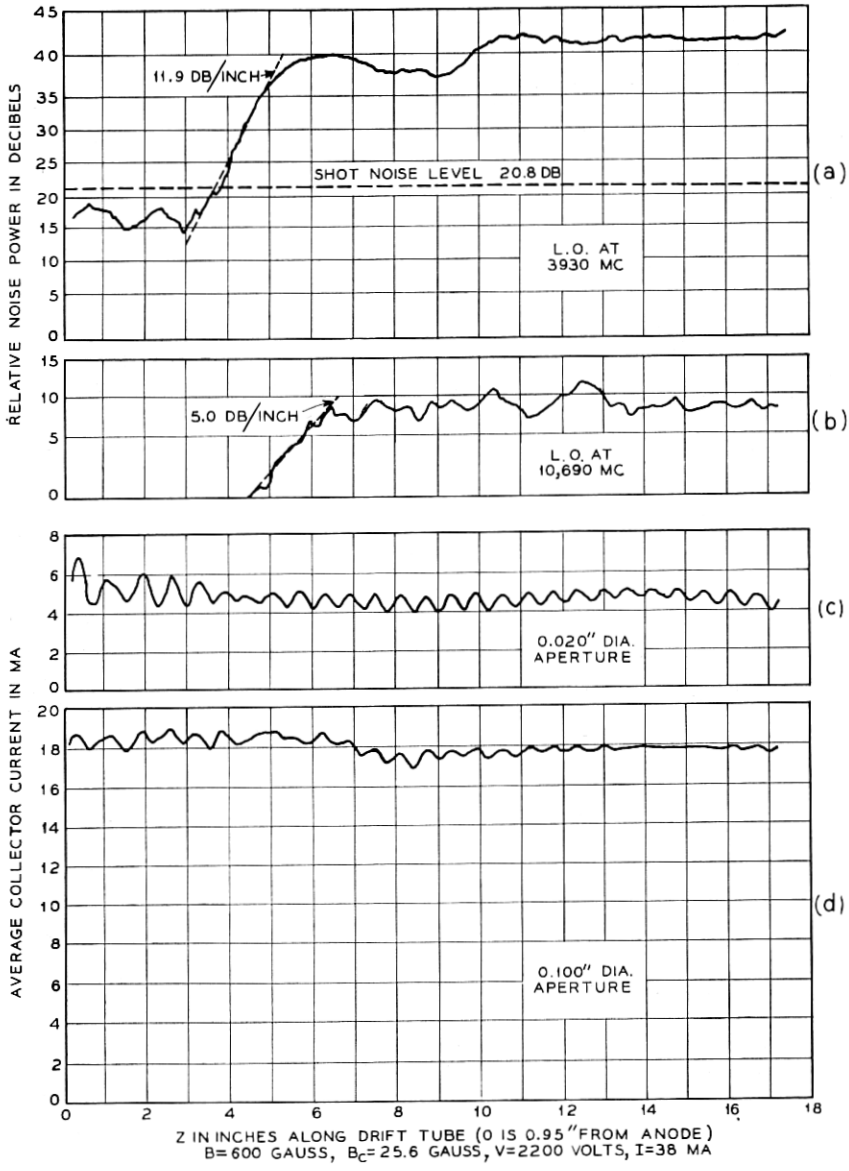

FIG. 2 — Typical smooth steep growing-noise patterns, near 4 and 10.7 kmc, respectively, with customary focusing field of about four times the Brillouin value. Collector-current traces through small and large apertures reveal decreases in ripple amplitude and increase in average beam diameter.

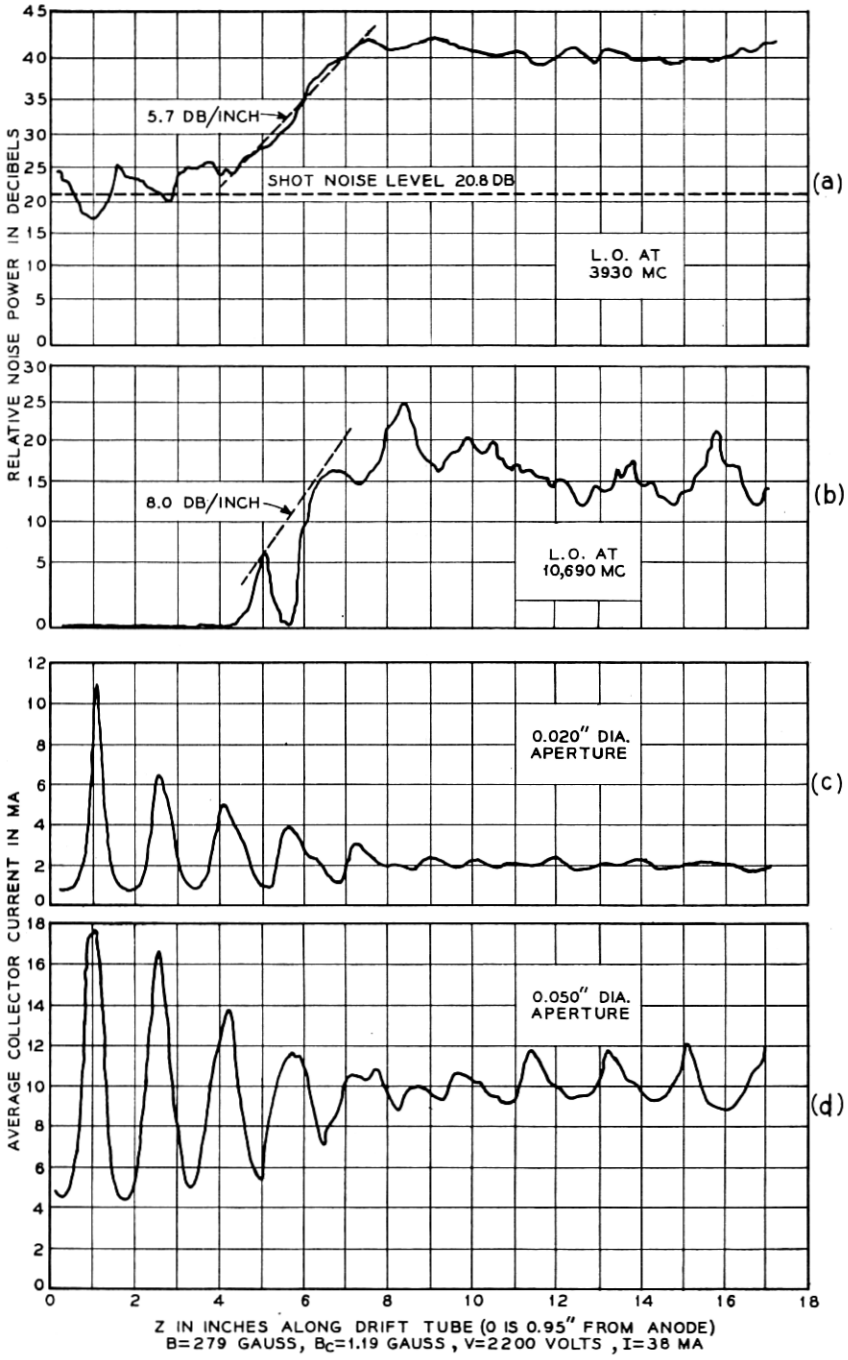

FIG. 3 — At about half the focusing fields used in Fig. 2, the growing-noise pattern is much the same at 4 kmc, but shows significant articulation at 10.7 kmc. The collector-current traces show pronounced decreases in ripple amplitude, and differences in ripple patterns obtained with different apertures.

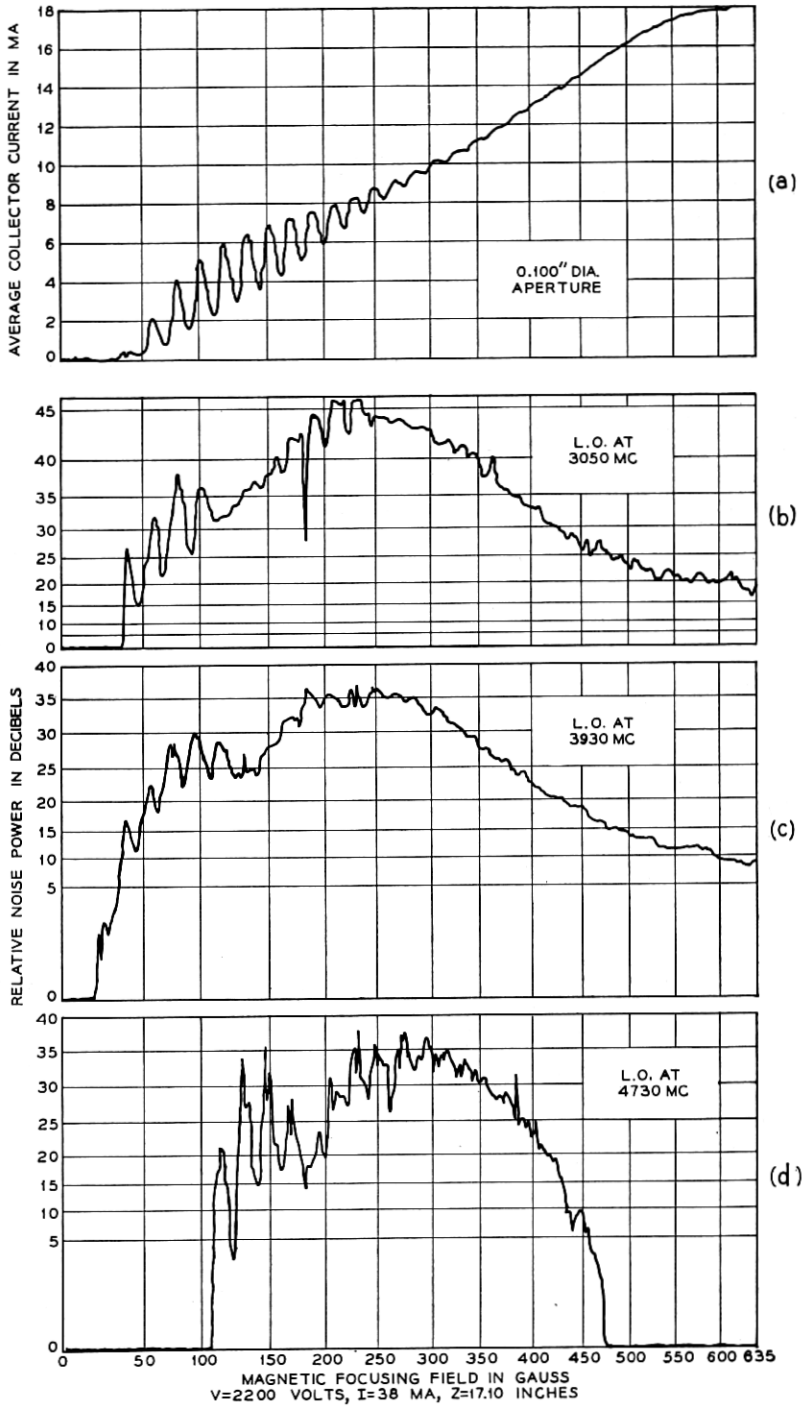

FIG. 4 — With the probe stationary at about 18 inches from gun anode, collector current and noise powers in bands about 1 kmc apart are recorded, as current in the main solenoid is varied from 0 to 1.5 amperes (0 to 635 gauss).

(2) The lower the frequency, the lower the field strengths at which noise amplitudes change most violently with field.

(3) The three noise curves resemble each other in small details.

The results of a great many records of the kind illustrated by Figs. 2 and 3 can be summarized as follows:

(1) There is always a decrease in beam-ripple amplitude associated with noise growth at any frequency. (Sometimes the ripple amplitude increases afterwards, as in Fig. 3.)

(2) The higher the frequency, for a given field, the more articulated or scalloped the noise pattern.

(3) No correlation can be found between rate of noise growth and either (a) distance from gun to take-off plane, or (b) net gain at the end of the drift region. The trends, as a function of magnetic field, are different at different frequencies.

(4) Greatest noise growth does not, as a rule, occur with zero flux threading the cathode. Sometimes two nearly equal peaks occur for two values of B_c, each of opposite polarity, referred to the sense of the main field.

(5) The noise-distance patterns change very slowly with frequency.

(6) No beam entirely ripple-free throughout its length has ever been observed by the writer.

IV ORIGIN OF GROWING NOISE

If noise growth is due to some amplification process, it should be possible to adjust the beam-focusing conditions so that the noise currents start increasing at the anode, and attain the greatest possible over-all gain at the end of the drift space. The enhanced activity of the unknown gain mechanism should presumably help identify it. The curves of Fig. 4 show that maximum noise occurs at different values of the focusing field, for different values of field at the cathode, and different probe positions. With the anode voltage and receiver frequency fixed, therefore, the conditions for greatest net noise growth can only be found by a series of trial settings of *both* magnetic fields, each followed by a recording of the noise-distance pattern. Eventually, a set of fields can be found for which the greatest total gain occurs; and such patterns are usually found to show fairly steady noise-amplitude increase, on the average, over the entire length of probe travel.

The results of this procedure for noise power near 4 kmc, as well as the patterns of collector-current versus distance with the same fields, using the 0.100-, 0.050-, and 0.020-inch apertures fixed at the probe centerline, are shown in Fig. 5. A similar set of records, for noise power

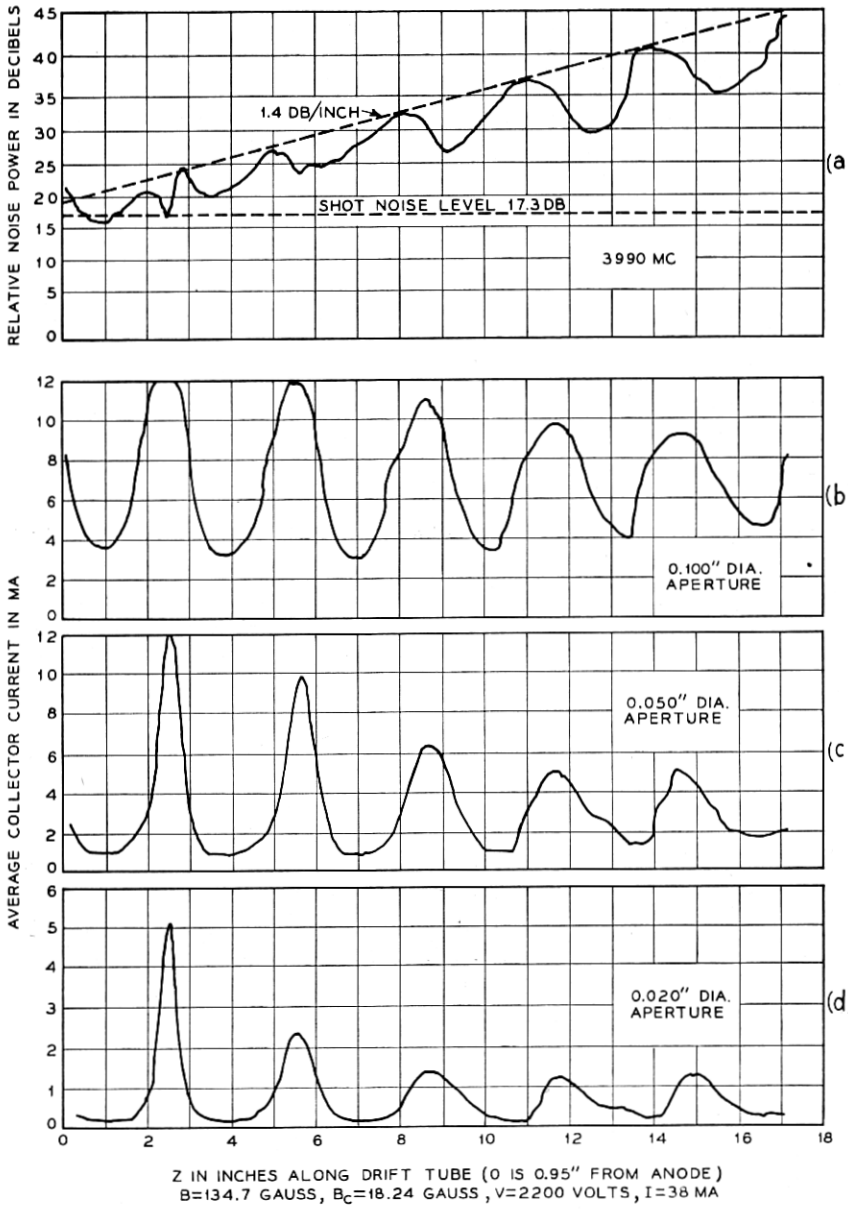

FIG. 5 — The magnetic fields in drift tube and at the cathode have been adjusted empirically to expand the growing-noise region over the entire drift region, with the L.O. at 3,990 mc. The field is slightly less than the Brillouin value, but the beam is strongly rippled because the gun was designed for best focusing at a much higher field. The noise-current maxima align with the average collector currents on their increasing slopes, for all three aperture sizes.

near 10.69 kmc, is shown in Fig. 6. The significant features of both sets of records can be summarized as follows:

(1) In both cases, the beam-ripple periods are equal to the *RF* scallop periods; i.e., the half-wavelengths of the space-charge standing waves. The noise minima tend to occur at planes where the collector currents are at their average values and decreasing; i.e., where the beam diameters are at their average values and increasing. The noise-current maxima occur where the beam diameters are about to decrease. These are the classical conditions for *rippled-beam amplification*.[6, 7, 8]

(2) In Fig. 5, the ripple amplitudes and peak values of all three collector-current curves decline appreciably with distance, the rate of decline being greatest for the smallest aperture. (Similar curves, not shown here, have displayed little or no such decline in the absence of noise growth.) This suggests that the RF noise power is amplified at the expense of dc energy associated with radially-directed electron velocities.

(3) In Fig. 6, the disparity among rates of decline of current-ripple amplitudes and their peak values, for the three aperture sizes, is even more pronounced. In addition, the ripple wavelength barely changes for the 0.100-inch aperture, but increases with drift distance for the smaller apertures, resulting in an increasing "phase shift" among them. Thus the current-density variations at different radii in the beam can contribute unequally to space-charge wave amplification, depending on their local ripple amplitude and phase. In this instance, the variations in current density along the beam are initially greatest near the axis, and suffer the greatest reduction there. It is worth noting that this "inner rippling" would be missed entirely in beam-size measurements with a large aperture.*

The decrease of beam ripple and the increase in average beam diameter, shown in Figs. 5 and 6, has been found to accompany rippled-beam amplification of impressed signals by T. G. Mihran.[8] Another corroboration of the identity of this gain mechanism can be obtained by comparing the measured noise gain per scallop with that predicted by theory for idealized conditions.[6, 7] For a beam with stepwise alternations of maximum and minimum beam diameters (ratio r_2/r_1), and with noise maxima and beam-diameter maxima coinciding, the gain per scallop is as follows:

$$G_m = \left(\frac{V_1}{V_2}\right)^{3/4} \left(\frac{r_2}{r_1}\right) \left(\frac{p_1}{p_2}\right). \tag{1}$$

Here, V is the beam potential, and p the reduction factor ω_q/ω_p. Although the actual rippled beam is far removed from either Brillouin or

* More information about "inner rippling" will be presented in Part II.

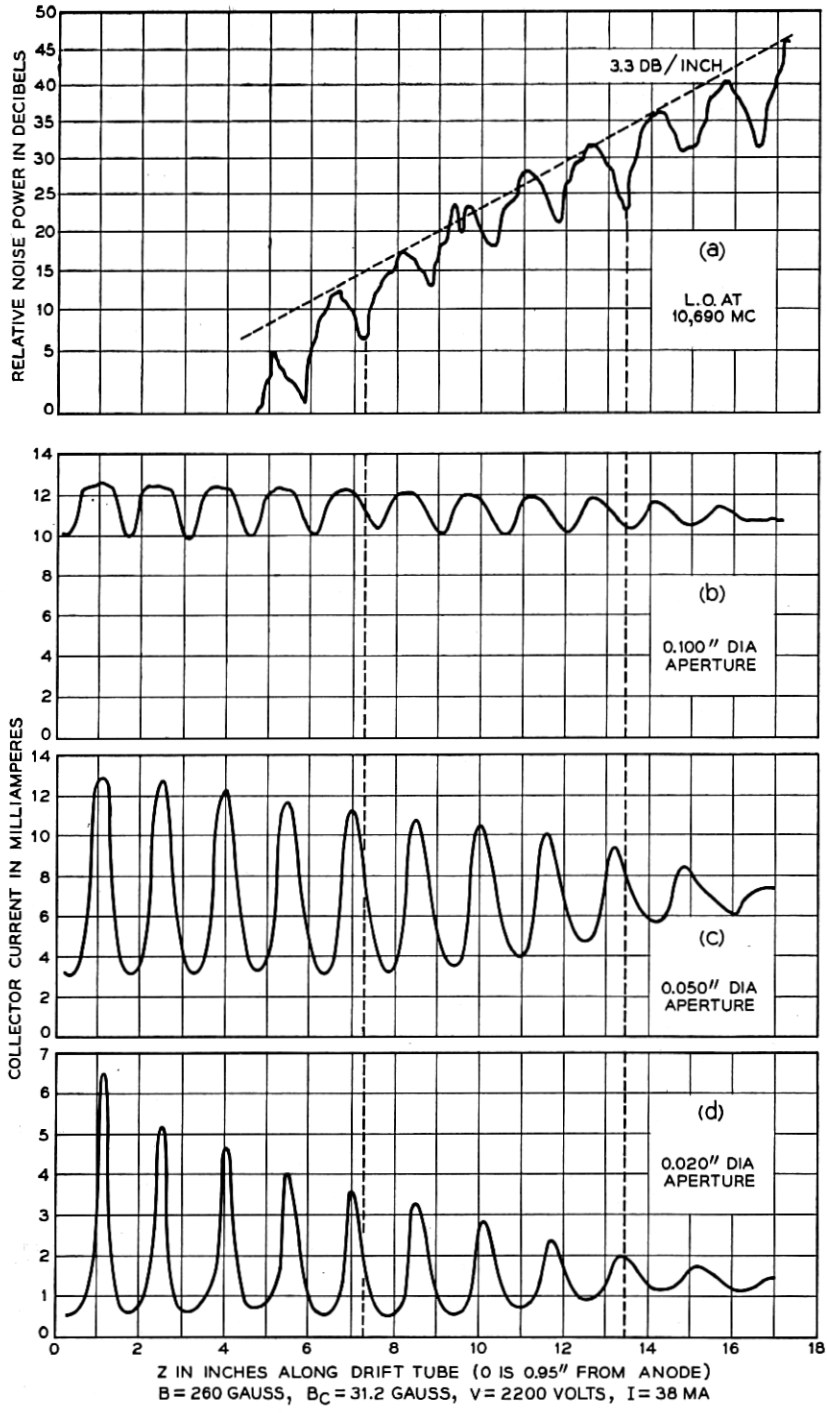

FIG. 6 — The fields have been adjusted as in Fig. 5, for maximum extension of the gain region, for noise power near 10,690 mc. Collector current measured with the smallest aperture shows the greatest decline in amplitude of variations, as well as advance in ripple phase relative to the current through the largest aperture.

TABLE I — MEASURED VERSUS CALCULATED MAXIMUM NOISE GAIN

Freq. mc.	Ripple Data		Gain in db per Scallop		
	Iris Dia. Inches	r_2/r_1	Brillouin Flow	Confined Flow	Measured
3,990	0.020	3.4	6.1	5.0	4.3
	0.050	3.2	6.3	5.4	
	0.100	1.9	4.0	3.3	
10,690	0.020	2.5	6.4	5.6	4.9
	0.050	1.8	4.8	4.4	
	0.100	1.1	<1.0	<1.0	

confined flow, the published values of reduction factor for both extremes can be used as first approximations.[10, 11] The ratio r_2/r_1 can be estimated by assuming the current density to be uniform over the beam cross-section near the middle of the drift region, for each of the three apertures used. The potential variations can be neglected. The results of such calculations are given in Table I.

As the computed gains are expected to be somewhat greater than those measured, because of the optimum conditions assumed, the best correspondence between measured and computed gain rates appears to be for the ripple data taken with the 0.050-inch iris at 3,990 mc, and that with the 0.020-inch iris at 10,690 mc. This distinction is in accord with previous qualitative comparison of Figs. 5 and 6, showing that most of the beam cooperates in the ripples of the former, but that "inner rippling" characterizes the latter.

Another calculation that reveals which part of the beam is interacting with the RF noise field in each case is that of the space-charge half-wavelength, as follows:

$$\frac{\lambda_s}{2} \cong \frac{\pi b}{p \cdot \beta_p b}, \tag{2}$$

where

$$\beta_p b = 174 I^{1/2}/V^{3/4}. \tag{3}$$

Here β_p is the plasma wave number, b the beam radius, and p the reduction factor, which can be evaluated as previously for the smooth beam in either ideal Brillouin or confined flow. For the gun used here, the square root of the perveance is

$$I^{1/2}/V^{3/4} = 0.606 \times 10^{-3} \text{ MKS units},$$

or

$$\lambda_s/2 \cong 29.8\, b/p. \tag{4}$$

TABLE II — MEASURED VERSUS CALCULATED SPACE-CHARGE HALF-WAVELENGTHS

Freq. mc.	Iris used, inches dia.	Avg. beam radius r_0 inches	γ rad./in.	$\lambda_s/2$, inches			Ripple Wavelength L, meas'd
				Brillouin Flow	Confined Flow	Meas'd	
3,990	0.050	0.057	22.9	3.2	2.7	3.0	3.06
10,690	0.020	0.033	61.2	1.6	1.3	1.47	1.52

Thus, agreement between this expression and the measured value requires the correct choice of the effective beam radius, b. It turns out that the suitable value for Fig. 5 (3,990 mc) is the average beam radius obtained from ripple data taken with the 0.050-inch iris, and that for Fig. 6 (10,690 mc) is obtained with data taken with the 0.020-inch iris. The results are summarized in Table II.

With this mechanism as the primary source of the noise gain, it becomes clear why nearly equal noise maxima were found, with some values of the main focusing field, B, for two values of cathode flux density B_c of opposite polarity. From approximate analyses of beam ripples when flux threads the cathode, such as those provided by McDowell[12] and others, it is found that the ripple wavelength depends nearly altogether on B. Its amplitude and spatial phase, however, depend on B_c, as this affects the beam geometry at the drift-space entrance. For a sufficiently wide range of variation of B_c, the spatial phase of the ripples can be varied from the proper relation with the space-charge standing wave for gain, through the positions for de-amplification, and back to gain again.

V THE GROWING-NOISE MECHANISM

Although many earlier noise records can be understood in the light of the rippled-beam amplification (RBA) process, this is not yet true of the smooth, steep noise growth usually observed, as in Figs. 2 and 3. The simple theory predicts that a space-charge wave will be amplified when, for small ripples, a "resonance" condition exists between the ripple wavelength, L, and the space-charge half-wavelength

$$L \cong n\lambda_s/2, \tag{5}$$

where n is an integer, usually unity. In addition, as mentioned earlier, there is an optimum phase relation between ripple and standing wave for maximum gain. These conditions are not satisfied by the records of

Figs. 2 and 3, except possibly for the 10.7 kmc noise current in Fig. 3 (at a relatively low magnetic field).

To establish a connection between the two types of noise growth, the noise record of Fig. 6 (for 10.7 kmc with greatly expanded gain region) is compared with that near 4 kmc under the same conditions, in Fig. 7. The growing noise region for 4 kmc does not start until at least four scallop wavelengths past the earliest observed 10.7 kmc noise growth. Moreover, the 4-kmc noise pattern resembles that for 10.7 kmc in many details. (The resemblance in details of noise patterns at nearby frequencies has been remarked before, in connection with Fig. 4.)

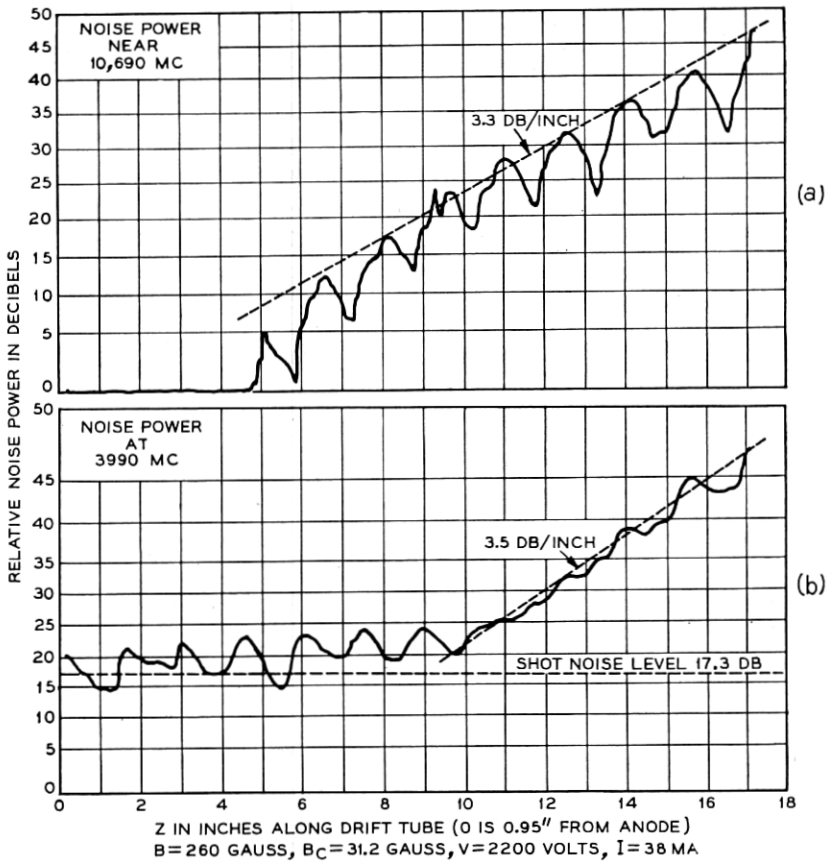

FIG. 7 — The pattern of growing noise in Fig. 6, near 10,690 mcs, is compared with that near 3990 mc for the same fields. The gain region of the latter curve starts much later and is much smoother than the former. The small irregularities on the 3,990 mc curve resemble the scallops of the 10,690 mc curve, in a blurred way.

This information suggests that the growing-noise mechanism is really a two-stage process: amplification of a broad band of microwave frequencies, located far above the observation frequency, followed by a transfer of noise energy to lower frequencies.

(*a*) *First stage*

At low magnetic fields, there are few ripples per unit length, but their amplitude is usually large; whereas at moderate to large magnetic fields, the ripple amplitude is small, but so is the ripple wavelength. In either case, the bandwidth of RBA is large, usually many thousands of megacycles.

The increase of both bandwidth and gain per scallop with ripple amplitude has been explained by Pierce[13] by analogy between the gain band of a rippled beam and the stop band of a transmission line filter: a sharply varying periodic disturbance on the latter will reflect short as well as long waves, whereas smoother perturbations will not reflect the shorter waves to any extent.

Another way to study the amplification bandwidth is to derive the equations for RF current in a one-dimensional beam with sinusoidal variation of the reduced plasma wave number, $\beta_q = p \cdot \beta_p$, as Heffner,[14] Bloom,[15] and others[16, 17] have done. This leads to a Mathieu equation, whose solutions may be studied on the Mathieu stability plot (A, q):

$$\frac{d^2I}{dx^2} + (A - 2q \cos 2x)I = 0. \tag{6}$$

Here I is the RF current, q a measure of the perturbation amplitude, $x = \pi z/L$, and $A = (2L/\lambda_q)^2$, where L is the ripple wavelength and λ_q the reduced plasma wavelength. Bloom has shown that, if n is the integral number of scallop wavelengths between initial and final planes, the greater the *product* nq, the greater the total amplification or deamplification, and the less critical the phase relation between RF standing wave and ripple for amplification. Ultimately, for very large nq, amplification will take place for all values of this phase angle.

At higher magnetic fields, both the ripple amplitude and ripple wavelength are decreased. This means that q is reduced, but n increased over any fixed span. This combination usually tends to increase the product nq up to some fairly high field, after which it may decline. More important, the reduction in ripple wavelength shifts the band of amplification to higher frequencies, and greatly increases the frequency band. This occurs because the "resonant" space-charge wavelength is shorter,

and short space-charge wavelengths correspond to high frequencies, where the former change very slowly with frequency.

(*b*) *Second stage*

When noise power over this large band has been amplified sufficiently, electron bunching becomes non-sinusoidal, and the beam becomes non-linear. Harmonics and beat-frequencies[18] of the fundamentals, and possibly sub-harmonics,[19] are excited. As the beat-frequencies are excited by a continuum of pairs of frequencies, their standing-wave patterns overlap one another, resulting in a "wash-out" of the noise minima, and a smooth growing-noise pattern. Eventually, the same non-linear processes take place within this subsidiary band, leading to a gradual leveling of the entire noise spectrum. The *initial* rates of rise of the intermodulation products, however, should take place closer to the gun and be greater, for a *lower* frequency. They will depend on both the spectrum of noise power in the primary band and, so to speak, the spectrum of "beam non-linearity" within that band.

To simulate this intermodulation process, two low-level klystron signals (9,050 and 12,275 mc, respectively) were simultaneously permitted to modulate the electron beam as it entered the drift tube, by means of a short length of lossy helix. The magnetic fields at the cathode and in the drift space were adjusted to produce a beam ripple which amplified both of these signals simultaneously over most of the drift space, as shown in Fig. 8 (a, b, c).* Noise-power records were then made at the difference-frequency, in the presence of the two modulation signals, Fig. 8(d), and in their absence, Fig. 8(e). The difference between the noise levels in the latter two records increases with distance, as both parent space-charge waves grow in amplitude, and the degree of beam non-linearity increases. Naturally, the contribution to 3,295-mc noise in the absence of modulating signals is far greater than that of the latter two alone, as the primary bandwidth of noise amplified is very great, and that of the signals very small.

There are several reasons why exponentially-growing noise should stop growing and level off, and sometimes even decrease slightly:

(1) depletion of dc kinetic energy in the beam ripples;

(2) de-amplification in the fundamental band, due to departure from the proper phase relation for gain between standing wave and ripple, if only over part of the band (Fig. 3);

* The fine ac detail superimposed on the pattern of Fig. 8(b) is due to interference between the waves traveling along the beam and that propagating as a waveguide mode in the drift space.

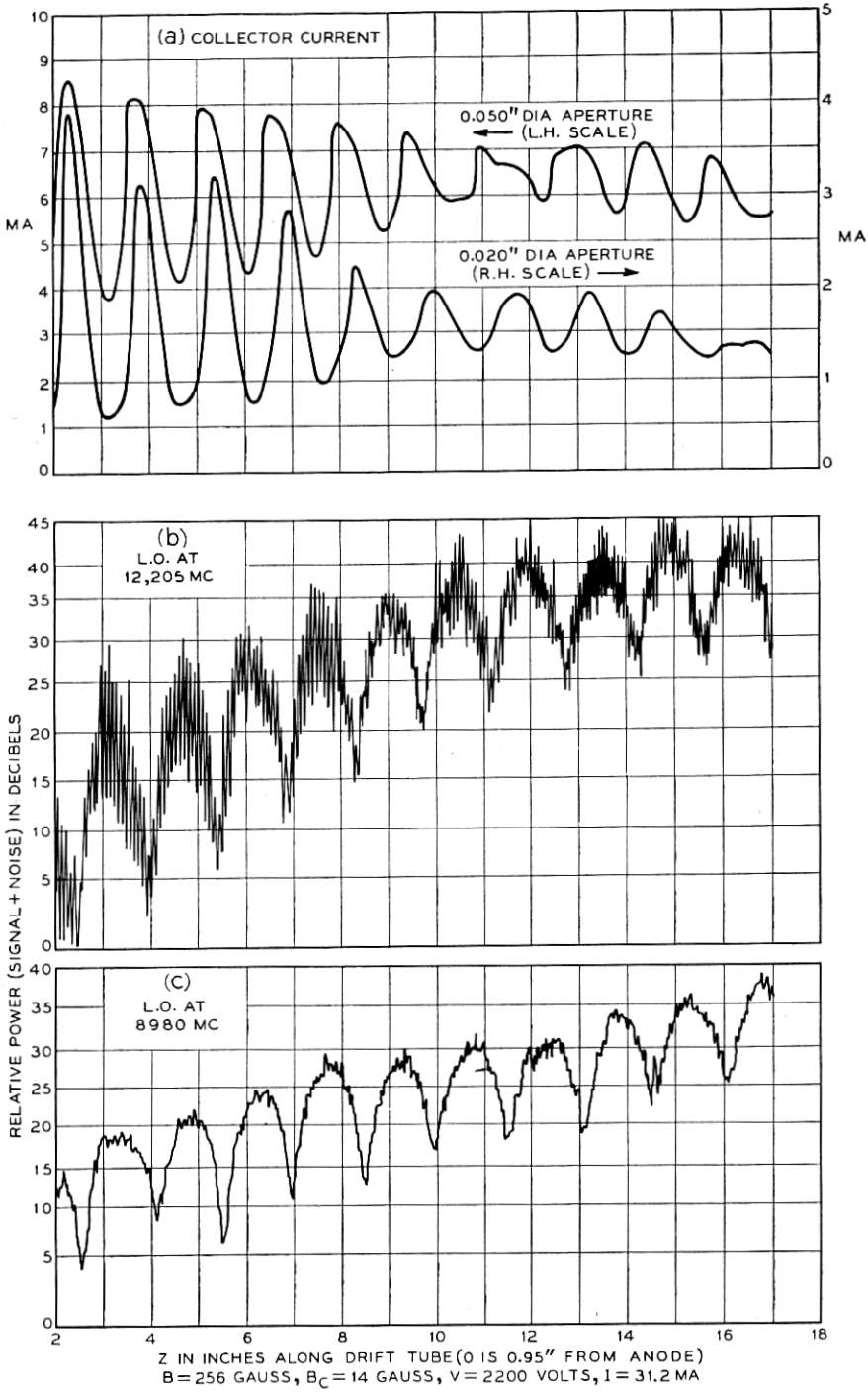

FIG. 8 (a), (b), (c) — The fields have been adjusted to give rippled-beam amplification of two weak klystron signals, 12,275 and 9,050 mc, simultaneously impressed on the beam at the entrance to the drift region.

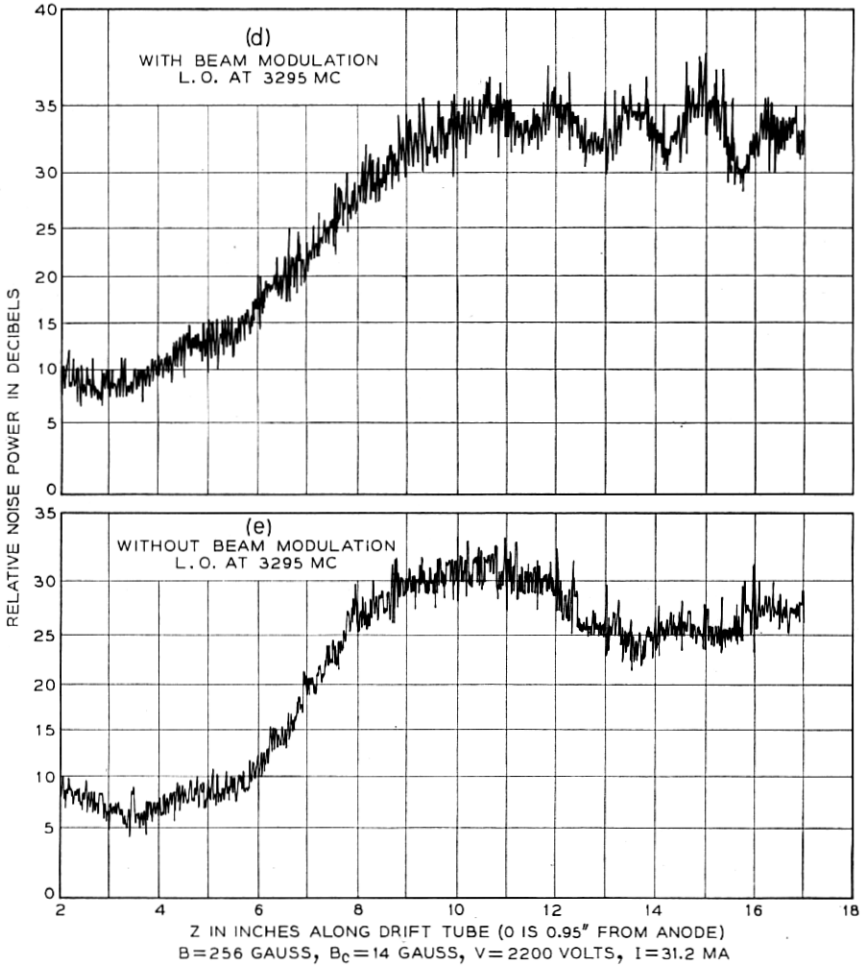

FIG. 8 (d), (e) — Noise power at the difference-frequency, 3,225 mc, is recorded, with and without the signals (b) and (c) present. The difference in ordinates of the two curves increases with distance from the gun, as the impressed signals grow and the beam becomes more non-linear.

(3) sufficient phase shift between inner and outer ripples in the beam for one to de-amplify as much as the other amplifies; and

(4) interference among the intermodulation products excited at different positions along the beam.*

The last effect is illustrated in Fig. 9, in exaggerated form. The beam

* Suggested by C. C. Cutler of Bell Telephone Laboratories.

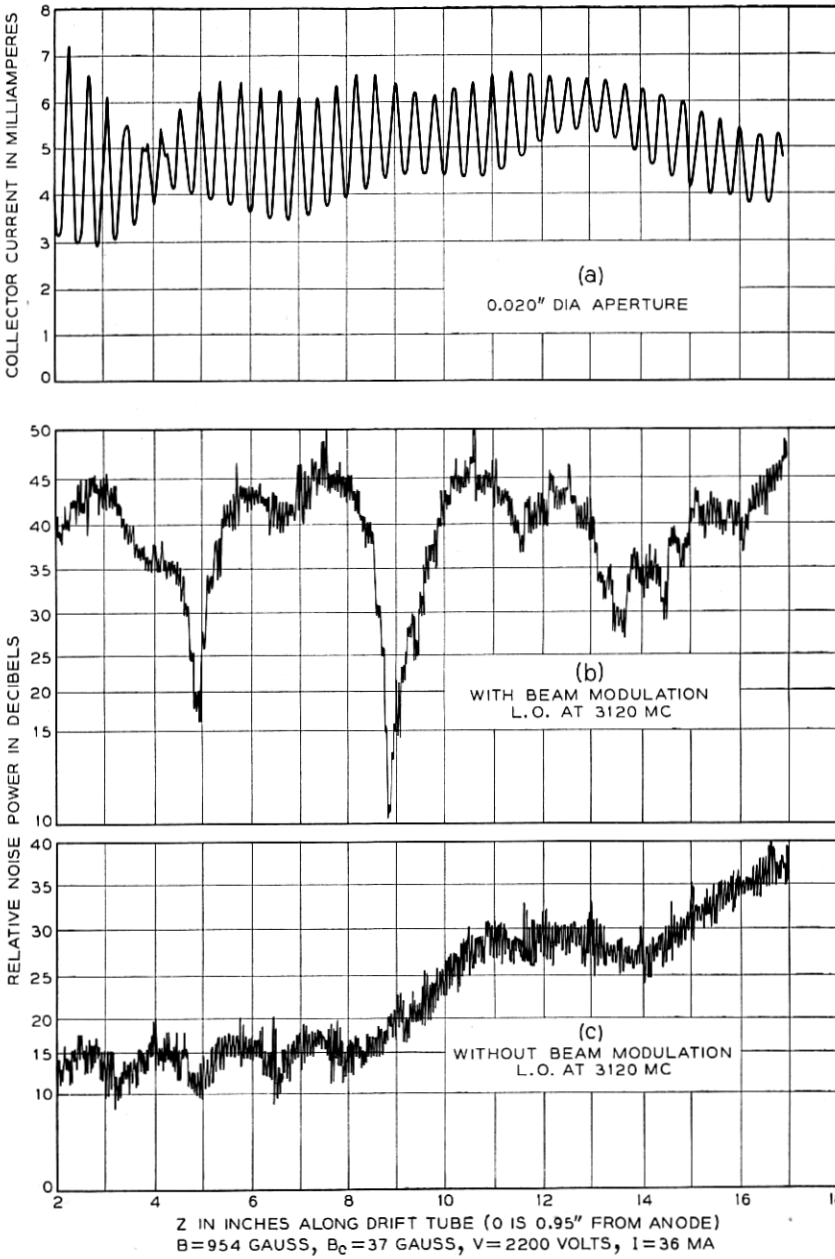

FIG. 9 — Two strong klystron signals are impressed on the beam as in Fig. 8, and noise power at their difference-frequency recorded, both with and without these signals present. The deep noise minima in (b) are due to destructive interference between trains of waves excited by intermodulation at different positions along the beam.

is simultaneously modulated as before with two klystron signals (8,400 and 11, 590 mc, respectively), but now at fairly high level; and the focusing field is made large. The interference dips in the pattern of 3,120-mc noise are quite deep, and are spaced irregularly and farther apart than the space-charge wavelength of any of the three frequencies involved. The third dip is shallower than the previous two because of the growth of 3,120-mc noise other than that due to the signals, as shown in Fig. 9(c). The latter pattern of noise in the absence of the two high-level, high-frequency signals suggests that the characteristic first gentle dip following the growing-noise region is indeed of the same nature as the artificially-produced interference dips, and has nearly the same quasi-period.

The pattern of dips agrees with simple calculations, based on this model, in which the amplitude of the difference-frequency intermodulation product, excited at any plane ζ, is assumed proportional to the product of the amplitudes of the two high-frequency space-charge standing waves, as follows:

$$| di_3 | \propto | i_1(\zeta) \cdot i_2(\zeta)\, d\zeta |, \tag{7}$$

where

$$i_n = I_n \sin p_n \beta_p \zeta \cdot \sin \omega_n (t - \zeta/u), \qquad (n = 1, 2).$$

The total current at $\zeta = z$ is the sum of contributions from all the standing waves excited to the left of it:

$$| i_3 | \propto \frac{1}{4} I_1 I_2 \int_0^z \cos p_3 \beta_p (z - \zeta)[\cos (p_1 - p_2)\beta_p \zeta - \cos (p_1 + p_2)\beta_p \zeta]\, d\zeta. \tag{8}$$

This expression is readily integrated and evaluated.

VI CONCLUSIONS

Synchronized measurements of electron-current density and noise currents at several microwave frequencies have shown that the "growing noise" pattern in drifting cylindrical beams is the result of a two-stage process. In the first stage, rippled-beam amplification of noise fluctuations takes place over a very broad band of microwave frequencies, much higher than the usual observation frequency. In the second, noise energy is transferred to lower frequencies by intermodulation and other non-linear processes within this band. The element of non-linearity is supplied when primary noise gain is sufficient to make electron bunching

non-sinusoidal. Other sources of non-linearity are thermal velocities, non-laminar beam flow, etc. As the beat-frequency noise increments at any plane are produced by continuous arrays of frequency pairs, increasing in numbers and amplitude in various ways as primary amplification proceeds, the multiple standing-wave patterns at the observation frequency progressively overlap one another. This results in the smooth steep rise of noise power usually observed.

Phase correlation among the space-charge waves excited at successive planes on the beam by the same set of frequency pairs is indicated by gentle dips, due to their destructive interference, in the plateau following the initial noise rise.

Rippled-beam amplification occurs whenever the ripple wavelength and half the space-charge wavelength are nearly equal, and bear a favorable spatial relation to each other. However, this "phase" relation becomes less critical with an increase in either the number of ripple wavelengths over which synchronism persists, or the ripple amplitude, or both. Noise amplification by this mechanism, therefore, is probably present to some degree in all rippled streams, particularly at high fields. The extreme difficulty encountered in focusing ripple-free beams from convergent, shielded guns has to this date prevented the detection of any other primary gain mechanism, which may conceivably co-exist in such beams.

A conspicuous feature of rippled-beam amplification is the decrease in ripple amplitude due to conversion of dc into ac kinetic energy. Such changes in beam structure emphasize the inadequacy of beam-flow computations based entirely on dc force equations. A more detailed description of this dc-ac energy conversion is given in Part II.

ACKNOWLEDGMENTS

The experimental apparatus could not have been built without the combined efforts of many associates of the writer, principally A. R. Strnad, P. Hannes, J. S. Hasiak and J. M. Dziedzic. The author is also indebted to R. Kompfner, C. F. Hempstead and K. M. Poole for valuable suggestions; and above all to C. F. Quate for constant encouragement and advice.

REFERENCES

1. C. C. Cutler and C. F. Quate, Experimental Verification of Space-Charge and Transit Time Reduction of Noise in Electron Beams, Phys. Rev., **80**, p. 875, 1950.
2. L. D. Smullin and C. Fried, Microwave Noise Measurements on Electron Beams, Trans. I.R.E. **ED-1**, No. 4, p. 168, Dec., 1954.

3. C. Fried, Noise in Electron Beams, Tech. Rep. 294, Research Laboratory of Electronics, M.I.T., May 2, 1955.
4. J. R. Pierce and L. R. Walker, Growing Waves Due to Transverse Velocities, B.S.T.J., **35,** p. 109, Jan., 1956.
5. G. G. Macfarlane and H. G. Hay, Wave Propagation in a Slipping Stream of Electrons: Small Amplitude Theory, Proc. Royal Soc. (B) **63,** p. 409, 1950.
6. C. K. Birdsall, Rippled Wall and Rippled Stream Amplifiers, Proc. I.R.E., **42,** p. 1628, Nov., 1954.
7. R. W. Peter, S. Bloom, and J. A. Ruetz, Space-Charge-Wave Amplification along an Electron Beam by Periodic Change of the Beam Impedance, RCA Rev., **15,** p. 113, March, 1954.
8. T. G. Mihran, Scalloped Beam Amplification, Trans. I.R.E., **ED-3,** No. 1, p. 32, Jan., 1956.
9. R. H. Dicke, The Measurement of Thermal Radiation at Microwave Frequencies, Rev. Sci. Instr. **17,** p. 268, July, 1946.
10. W. W. Rigrod and J. A. Lewis, Wave Propagation Along a Magnetically-Focused Cylindrical Electron Beam, B.S.T.J., **33,** p. 399, March, 1954.
11. G. M. Branch and T. G. Mihran, Plasma Frequency Reduction Factors in Electron Beams, I.R.E. Trans., **ED-2,** No. 2, 3, April, 1955.
12. Informal communication from H. L. McDowell.
13. Informal communication from J. R. Pierce.
14. Informal communication from H. Heffner.
15. S. Bloom, Space-Charge Waves in a Drifting, Scalloped Beam, unpublished RCA Research Laboratories report.
16. O. E. H. Rydbeck and B. Agdur, Propagation of Space-Charge Waves in Guides and Tubes with Periodic Structure, L'Onde Electrique, **34,** p. 499, June, 1954.
17. P. V. Bliokh and Y. B. Feinberg, Space-Charge Waves in Electron Beams with Variable Velocity, Zhurnal Tekhn. Fiziki, **26,** p. 530, March, 1956.
18. C. C. Cutler, The Nature of Power Saturation in Traveling Wave Tubes, B.S.T.J., **35,** p. 841, July, 1956.
19. S. Lundquist, Subharmonic Oscillations in a Nonlinear System with Positive Damping, Quarterly of Appl. Math., **13,** No. 3, p. 305, Oct., 1955.